Egypt. J. Chem. **Vol. 67,** No. 4 pp. 55 - 63 (2024)

Egyptian Journal of Chemistry

http://ejchem.journals.ekb.eg/

Physical Characterization of Indonesian Eri Silk Fiber Derived from Novel Strains of *Samia cynthia ricini*

Marlin Putri Maldia[1], Noviyan Darmawan[2] , Yuni Cahya Endrawati[3], Irma Herawati Suparto[1], Firda Aulya Syamani [4], Ronny Rachman Noor[5]

[1] *Department of Chemistry, Faculty of Math and Natural Science, IPB University, Jl. Tanjung Kampus IPB Dramaga Bogor, West Java 16680, Indonesia*

[2] *Department of Chemistry, IPB University Indonesia*

[3] *Department of Animal Science and Technology, Faculty of Animal Science, IPB University*

[4] *Research Center for Biomass and Bioproducts, National Research and Innovation Agency (BRIN), Jalan Raya Bogor Km. 46, Cibinong, Bogor, West Java 16911, Indonesia*

[5] *Department of Animal Production and Technology, Faculty of Animal Science, IPB University, Jl. Agatis Kampus IPB Dramaga Bogor, West Java 16680, Indonesia*

Abstract

Eri silk fibers are produced by the silkworm *Samia cynthia ricini,* which has been extensively cultivated in several tropical countries due to its adaptability to elevated temperatures and humidity, as well as the ample availability of its food sources. Currently, we have developed six new strains of *S. ricini* with extraordinary cocoon productivity and the ability to survive in marginal/extreme areas (high temperature and low humidity), namely Joglo, Jopati, Pasopati, Prasojo, Progo, and Tawang strains, respectively. This research analyzes the physical characterization of these Eri silk fibers, including the thermal characteristics, crystallinity structure, morphology, and functional groups of the silk fibers. The surface morphology of the degummed Eri silk fibers reveals the presence of separated fiber filaments with a smooth surface, ranging in diameter from 14 – 33 µm. The tensile strength and elongation of the silk fibers from the new strains do not show a significant difference ($P > 0.05$ %), around 350 – 497 MPa and 15 – 26 %, respectively. In addition, the Fourier transform infrared spectrometer was also utilized to investigate the structural differences of Eri silk fibers. The results show absorption bands at 1623 cm^{-1}, 1513 cm^{-1}, 1219 cm^{-1}, and 703 cm^{-1} indicating vibration of C=O (Amide I), N–H (Amide II), and C–N (Amide III) groups indicate the presence of β-sheet structures in the silk fibers. X-ray diffractograms of Eri silk fibers show peaks at 16.54° and 20.40° that correspond to the β-sheet crystalline structure. The new strain fibers have no significant structural disparities compared to the general *S. ricini* silk fibers. The thermal characteristics of the Eri silk fibers from the new strains are similar, with water removal occurring at temperatures around 100 to 125 °C and degradation temperatures around 369 – 373 °C. However, the Pasopati strain exhibits the highest heat capacity increment (ΔC_p), 1.266 J g^{-1} $°C^{-1}$. Based on the comparative results, Eri silk fiber from novel strains of *S. ricini* reported can be utilized more extensively in the textile industry and biomaterial applications.

Keywords: Eri silk, physical characterization, novel strain, *Samia cynthia ricini*

1. Introduction

The Eri silk fiber, also known as 'peace silk', is produced by the Eri silkworm (*Samia cynthia ricini*), it has a non-lustrous, robust, durable, and fine texture [1]. Eri silk fiber's fineness ranging from 14 to 16 microns is very close to wool fibers which can easily be blended with wool [2]. Eri silk exhibits heat resistance and water absorption capabilities, enabling it to provide warmth in cold weather and a cooling effect in hot weather [1]. Eri silk is widely used in the textile and clothing industry as a raw material for scarves, jackets, blankets, and other products [3]. In recent years, researchers have explored the potential of Eri silk in biomaterial applications such as drug delivery, wound healing, and tissue engineering

*Corresponding author e-mail: y-cahya@apps.ipb.ac.id
Receive Date: 04 July 2023, Revise Date: 17 August 2023, Accept Date: 14 October 2023
DOI: 10.21608/EJCHEM.2023.220190.8212

scaffolds [4]. The global silk market was valued at around USD 24.83 billion by the end of 2022 and is estimated to exhibit a compound annual growth rate (CAGR) of around 11.32% until 2028 [5]

Eri silkworm is well-suited for cultivation in tropical climates such as India, Thailand, and Indonesia compared to *Bombyx mori*, due to their adaptability to temperature, humidity, and food availability. Among all the silkworms, the Eri silkworm is hardy and more tolerant to temperature and humidity fluctuations [6]. It feeds on various host plants that can grow throughout the season such as Castor, Kesseru, and Tapioca [7]. However, climate change can impact Eri silkworm production, leading to unstable productivity under extreme conditions [8]. Moreover, the diverse topography of Indonesia contributes to environmental heterogeneity, characterized by variations in temperature and humidity [9]. Consequently, the emergence of novel silkworm strains, endowed with enhanced resistance to extreme conditions, coupled with the production of high-quality fibers that adhere to quality standards, becomes imperative.

Our previous studies have obtained six new strains: Joglo, Jopati, Pasopati, Prasojo, Progo, and Tawang [10]. These strains are resistant to environmental stresses, especially high temperatures and low humidity. Furthermore, the new strains' life cycle is faster than other Eri silkworm strains (39 to 45 days), which can increase fiber productivity. Studies show that silkworm strains can influence the properties and quality of the fibers [11]. Based on these considerations, a study was conducted on the physical characterization of the fibers from the six new silkworm strains, including mechanical properties, thermal characteristics, crystallinity structure, morphology, and functional groups.

Structurally, silk fibers consist of fibroin protein fibers coated with sericin as an adhesive [12]. When applied as textiles, sericin needs to be removed as it can affect the quality and application of the fibers [13]. This process is known as degumming. After degumming, the fiber morphology is observed using a scanning electron microscope (SEM) to ensure the absence of sericin [14]. One of the quality parameters of silk fibers is their mechanical properties, which can be measured using a universal testing machine (UTM), including tensile strength, strain, stress, and elongation [11]. Mechanical properties play a crucial role in the functionality and durability of the material in various applications [15]. The mechanical properties of silk are determined by its hierarchical structure, including factors such as the level of crystallinity, dimensions, and arrangement of crystallites, as well as the molecular-level conformation and orientation of polypeptide chains [16].

High-temperature exposure is often involved in handling, processing, and utilizing silk fibers. Therefore, understanding the heat resistance of the fibers is essential to prevent quality degradation. Thermal analysis methods, such as differential scanning calorimetry (DSC), are employed to identify the glass transition temperature (T_g), heat capacity increase at T_g, and thermal degradation of silk fibers. Thermogravimetric analysis (TGA) is also utilized to determine the moisture content and thermal degradation mechanisms of different silk fibers [17].

2. Experimental

The primary material used in this study is silk fiber derived from six new strains of Eri silkworms reared in the Laboratory of Natural Silkworm, Faculty of Animal Science, IPB University. These strains, namely Joglo, Jopati, Pasopati, Prasojo, Progo, and Tawang, were maintained separately with a population of over 100 silkworms. Randomly selected cocoons were used for analysis. The silk fiber obtained from wild Eri silkworms, coded as *S. ricini*, was used as a control. The equipment utilized includes glassware, analytical balance, water bath, scanning electron microscope (SEM), universal testing machine (UTM), differential scanning calorimeter (DSC), thermogravimetric analyzer (TGA), Fourier transform infrared spectroscopy (FTIR), X-ray diffractometer (XRD), and ImageJ software.

2.1. Degumming

The cocoons were cleaned from floss and residual pupae. Subsequently, they were washed and dried for degumming. Cocoons were boiled in an aqueous solution of 0.02 M Na_2CO_3 at 70 °C for 30 minutes to remove sericin [18]. After the process, the silk fibers were cooled by rinsing them three times with distilled water. The silk fibers were air-dried overnight.

2.2. Morphology Analysis

The morphology of silk fibers was observed by Thermo Scientific Quattro S Field-Emission Scanning Electron Microscope using an electron high voltage of 1 kV. The fibers were analyzed using ImageJ software to determine the diameter of the silk fibers.

2.3. Mechanical Properties Analysis

The mechanical properties were analyzed according to the ASTM D638 standard using a Shimadzu AG-IS 10 kN Universal Testing Machine. Tensile testing was conducted using a 5 kN load cell at a crosshead speed of 1 mm s^{-1}.

2.4. Thermal Property Analysis

The thermal stability was analyzed using a Differential Scanning Calorimeter (DSC). A five mg sample was wrapped in aluminum foil. Before analysis, the DSC machine was programmed to heat the sample at a rate of 10 °C min^{-1}. The heating process ranged from -20 °C to 350 °C. Fiber degradation was determined using a thermogravimetric analyzer (TGA) with a heating rate of 10 °C min^{-1} under a nitrogen atmosphere, spanning from 25 °C to 500 °C.

2.5. FTIR Analysis

Functional groups of silk fiber were analyzed using PerkinElmer Fourier transform infrared spectroscopy with an attenuated total reflectance (ATR) accessory, the wavenumber range of 4000 – 400 cm^{-1}.

2.6. XRD Analysis

A Shimadzu-7000 X-ray Diffractometer measured the samples' wide-angle X-ray diffraction (XRD) patterns. The scanning range of 2θ was set between 10° and 60°, with a scan speed of 1° min^{-1}.

2.7. Data Analysis

The tensile strength and elongation data were analyzed using statistical software (Microsoft Excel of Microsoft 365). The one-way analysis of variance (ANOVA) was utilized to identify any statistically significant variations in the mean values of the tensile strength and elongation data at a 5% level of probability.

3. Result and Discussion

3.1. Mechanical Properties and Surface Morphology of Silk Fiber

The surface morphology of Eri silk fibers was observed using SEM revealable as filaments with an uneven and granular surface before degumming, while the Prasojo fibers exhibited a smoother surface with minimal granulation (Fig. 1d). Generally, before the degumming process, the surface of the silk fibers exhibited filaments enveloped by an outer layer of sericin, which was predominantly intact [19]. Occasionally, thin cracks or locally abraded regions could be observed on the sericin layer surrounding the fibers [20].

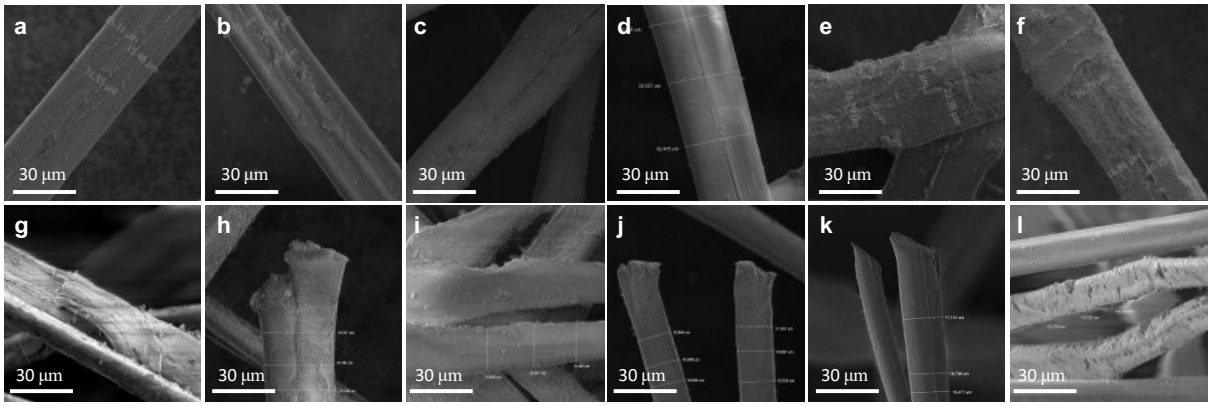

Fig. 1. Surface morphology of Indonesian Eri silk fiber derived from novel strains of *Samia cynthia ricini* before degumming (a-f) and after degumming (g-l) at a magnification of 3000x. The images illustrate the surface characteristics of the silk fibers from the Joglo (a,g), Jopati (b,h), Pasopati (c,i), Prasojo (d,j), Progo (e,k), and Tawang (f,l) strains

Table 1 The average diameter and mechanical properties of Indonesian Eri silk fiber derived from novel strains of *Samia cynthia ricini*

Silk fibers	Diameter (μm)	Tensile Strength (MPa)	Elongation (%)
S. ricini	20.33 ± 2.66	490 ± 12	32.16 ± 5.19
Joglo	24.09 ± 1.29	469 ± 21[a]	25.52 ± 5.80[a]
Jopati	33.14 ± 0.92	497 ± 24[a]	19.75 ± 0.85[a]
Pasopati	19.55 ± 1.04	427 ± 95[a]	15.17 ± 0.51[a]
Prasojo	16.64 ± 0.41	361 ± 136[a]	26.64 ± 7.22[a]
Progo	16.78 ± 0.33	350 ± 89[a]	19.44 ± 2.12[a]
Tawang	14.72 ± 0.39	435 ± 103[a]	23.16 ± 6.78[a]

Values followed by the same letter within a column are not significantly different from each other at a 5% level of probability

After degumming, silk fibers have a smooth surface composed of separated fibroin strands [12]. This appearance is consistent with the SEM results obtained for the Prasojo strain (Fig. 1j) and Progo strain (Fig. 1k), where separated fibroin strands with smooth surfaces are visible. In the Pasopati strain (Fig. 1i) and Tawang strain (Fig. 1l), the fibroin strands have separated, but there are still granules on the surface. Meanwhile, the fibroin strands are still fused and granular in the Joglo strain (Fig. 1g) and Jopati strain (Fig. 1h). This indicates that with the same degumming method, sericin removal efficiency is different for each silk fiber.

The fiber diameter and mechanical properties of Eri silk fiber are shown in Table 1. There are differences in diameter were observed among each strain. Differences in fiber diameter can affect the strength of the fiber because the tensile strength relies on the weakest point of the fiber, which is at the smallest diameter. The results of mechanical properties indicated that there is no statistically significant difference in the tensile strength and elongation ($P > 0.05$) among the new strains. These findings suggest that there is no variation in fiber quality among the new strains based on their mechanical properties.

However, it is essential to note that the new strains' tensile strength and elongation values were relatively lower compared to *S. ricini* and other research [16], indicating a decrease in fiber quality. It can be attributed to differences in the degumming methods employed. The degumming method influences sericin removal in silk fibers [21]. The study of the within-individual variation in the mechanical properties of Eri silk is essential for gaining insights into the relationship between silk structure and properties. Additionally, this investigation has implications for evaluating the diverse applications of silk [22].

*3.2. **Thermal Characteristics of Silk Fiber***

The thermal stability of different silk fiber samples was analyzed using DSC, and the scanning curves are shown in Fig. 2a. During heating, all samples exhibited a first peak around 25 – 110 °C, which was attributed to the water evaporation temperature (T_w) [23]. After the removal of water, a small peak (T_{d1}) appeared around 110 – 150 °C for all fiber strains except Jopati. The T_{d1} peak is an indicator of the degradation/melting of sericin [14]. Subsequently, the fibers maintained a stable heat flow without significant changes until the glass transition region (T_g).

All silk fibers showed heat capacity increments (ΔC_p) during the glass transition region, indicating a change from an amorphous to a crystalline state [24]. Based on the obtained results, it was found that Pasopati fiber exhibited a higher ΔC_p in the glass transition region compared to other strain fibers (Table 2). Meanwhile, the heat capacity of strain fibers tended to be higher than that of *S. ricini* fiber. The increase in heat capacity is directly proportional to the average protein chain mobility, reflecting the number of freely rotating bonds capable of altering chain formation [17]. After the glass transition region (T_g), all samples showed degradation peaks (T_{d2}) at temperatures ranging from 290 to 320 °C. This indicates minimal changes in crystallinity. The thermal degradation temperature of Eri silk fiber was higher than that of *B. mori* silk fiber (267 °C), indicating that Eri silk fiber had higher thermal stability than *B. mori* silk fiber [24].

The moisture content and thermal degradation of different silk fiber samples were analyzed using thermal gravimetric analysis (TGA). The thermogram in Fig. 2b shows the percentage mass change from

Table 2 Thermal data of Indonesian Eri silk fiber derived from novel strains of *Samia cynthia ricini*

Silk fibers	T_g (°C)	ΔC_p at T_g (J g^{-1} °C^{-1})	Moisture content (%)	T_d(°C)	Remaining mass at 450 °C (%)
S. ricini	200.26	0.874	9.123	369	47.765
Joglo	198.79	1.001	8.946	371	44.451
Jopati	195.84	0.794	9.630	373	42.587
Pasopati	204.63	1.266	9.004	370	45.881
Prasojo	200.84	1.235	8.658	369	47.186
Progo	201.11	1.015	7.686	368	49.920
Tawang	202.18	1.025	8.470	371	47.129

The first two columns (Glass Transition Temperature, Tg) and (Heat Capacity Increase, ΔCp) were determined by DSC analysis, while the rest were determined by TG analysis.

from room temperature to 500 °C during heating. Each sample experienced three main stages of mass loss. The first stage, from room temperature to 125 °C, exhibited a mass loss indicative of water evaporation, as observed in the DSC study. Water molecules form hydrogen bonds with the hydroxyl molecules in the silk chain structure, leading to the loss of absorbed water in this region [25]. The moisture content of the silk fibers is shown in Table 2, with varying amounts between the fibers, approximately 7 – 9 %.

The second stage, from 125 to 240 °C, represents a slow thermal degradation stage and the initial degradation temperature. This region indicates that all silk fibers exhibit good thermal stability, with no significant thermal degradation before 200 °C. The third stage, above 240 °C, represents the degradation process, where all silk fibers undergo rapid mass loss due to peptide bond cleavage and the breakdown of side chains of amino groups [26]. The degradation rate slows down after 450 °C, and no peak is displayed in the first derivative curve, allowing the determination of the remaining mass percentage of the silk fibers. The temperature range of 250 – 340 °C is associated with the degradation of amorphous silk [24], and the main peak at 370 °C is related to the degradation of β-sheet structures in the silk fibers [27].

The degradation process is further clarified in Fig. 2c, which depicts the first derivative of the remaining mass percentage. It is observed that the degradation temperatures between the new strain silk fibers and *S. ricini* are not significantly different. The degradation temperatures obtained in this study are close to those of Eri silk fibers reported in other regions, such as 359 °C for Eri silk from Kenya [14] and 369 °C for Eri silk from Bangalore [25]. Silk fibers with degradation temperatures above 300 °C indicate good orientation and crystalline structure [28].

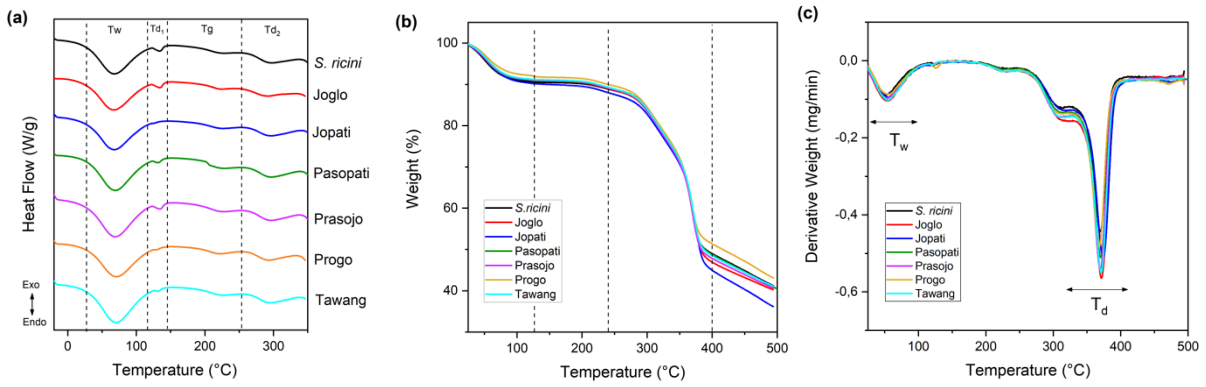

Fig. 2. (a) DSC scanning curves of different Eri silk fibers with temperature regions associated with water evaporation (T_w), glass transition (T_g), and sample degradation (T_{d1} and T_{d2}). (b) The remaining mass percentage of different Eri silk fibers was measured by TGA during heating from room temperature to 500 °C at a rate of 10 °C min^{-1}. (c) The first derivative of the mass percentage remaining depicts the degradation level of silk fiber and indicates temperature regions related to water evaporation (T_w) and sample degradation (T_d)

Table 3 Wavenumber (cm^{-1}) and functional groups of Indonesian Eri silk fiber derived from novel strains of *Samia cynthia ricini*

Silk fiber	Wavenumber (cm^{-1})				
	C=O *stretch*	N–H *bend*	C–N *stretch*	Ala-Ala	C–N *torsion*
S. ricini	1619	1512	1220	965	687
Joglo	1619	1513	1219	964	689
Jopati	1623	1513	1220	964	690
Pasopati	1624	1513	1220	964	691
Prasojo	1623	1513	1218	964	690
Progo	1622	1514	1218	964	684
Tawang	1624	1510	1218	964	690

3.3. *Functional Groups of Silk Fiber*

FTIR spectroscopy was carried out by identifying the functional groups of Eri silk fibers within the scanning range of 4000 – 500 cm^{-1}. FTIR spectroscopy is practical in the structural analysis of silk fibroin; the molecular conformation can be determined based on the position and intensity of the amide bands [29]. The FTIR spectra of each fiber are shown in Fig. 3 and the wavenumber data (cm^{-1}) is presented in Table 3.

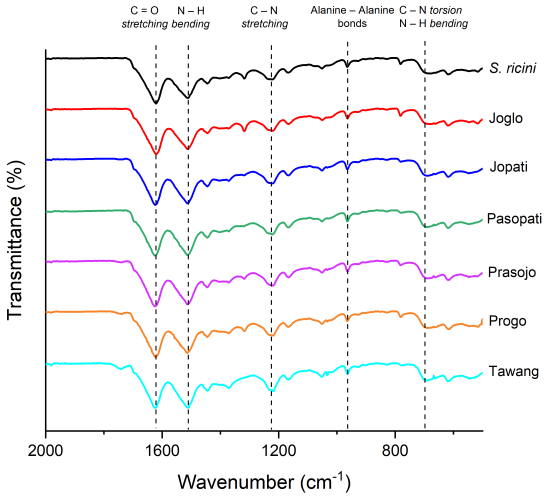

Fig. 3. FTIR spectrum of Indonesian Eri silk fiber derived from novel strains of *Samia cynthia ricini* in the scanning range of 2000 – 500 cm^{-1}

The peak around 1623 cm^{-1} is associated with the Amide I group (C=O stretching). The peak at 1513 cm^{-1} corresponds to Amide II (N-H bending). The peak around 1219 cm^{-1} corresponds to Amide III (C-N stretching). The peak around 964 cm^{-1} corresponds to the vibration of the Alanine-Alanine bond. The peak at 703 cm^{-1} corresponds to Amide V (C-N torsion and N-H bending). All the above peaks indicate the presence of β-sheet structures in the silk fibers. These peaks are observed at similar wavenumbers for Eri silk from Kenya [14]. Based on these findings, it can be concluded that there are no major structural differences between the Eri silk fibers, either among the different varieties or compared to *S. ricini* silk.

3.4. *X-Ray Diffraction of Silk Fiber*

X-ray diffraction (XRD) patterns were recorded to characterize Eri silk fibers and are shown in Fig. 4. Each silk fiber has two highest peaks at the diffraction angle (with its 2θ) of 16.9° and 20.5°. According to the classification used by Warwicker, Eri silk fibers fall into group 3a, which classifies β crystal fibroin. This validates the IR spectrum as there are characteristic peaks that correspond to the β-sheet crystalline structure[30].

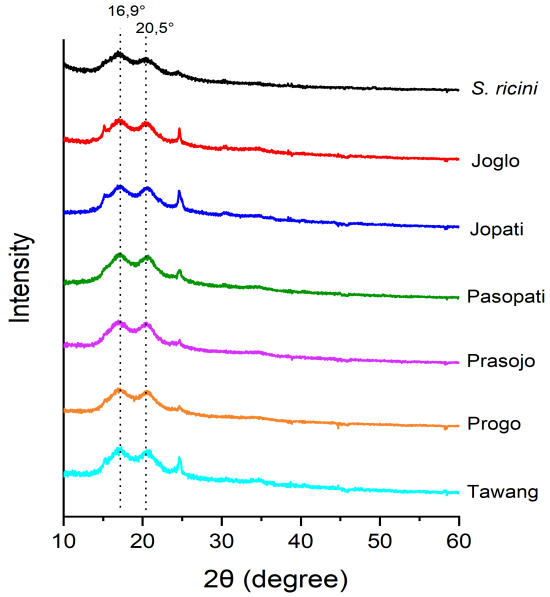

Fig. 4. X-ray diffraction pattern of Indonesian Eri silk fiber derived from novel strains of *Samia cynthia ricini*

Tabel 4 Crystallinity of Indonesian Eri silk fiber derived from novel strains of *Samia cynthia ricini*

Silk Fiber	Crystalline Region (%)	Amorphous Region (%)
S. ricini	18.2	81.8
Joglo	19.7	80.3
Jopati	18.4	81.6
Pasopati	10.1	89.9
Prasojo	14.2	85.8
Progo	13.4	86.6
Tawang	27.1	72.9

XRD pattern results also display the crystallinity of Eri silk fibers as shown in Table 4. There are variations in crystallinity among the different new strains, with Tawang silk fiber having the highest crystalline region at 27%, and Pasopati silk fiber having the lowest crystalline region at 10%. The crystallinity obtained in this study was lower than Eri silk fiber from Kenya at 29% [12]. The variations in crystallinity can be attributed to differences in genetic, environmental conditions, maintenance, and nutritional intake, which can lead to changes in the molecular structure, structural alignment, and protein composition within the silk fibers [31][32]. The degumming method also influences the crystallinity of silk fibers [33].

4. Conclusions

Indonesian Eri silk fiber derived from novel strains of *Samia cynthia ricini* shows variation in their mechanical properties and thermal characterization. However, the Pasopati strain exhibits the highest heat capacity increment (ΔC_p) compared to the other strains. No significant structural disparities are observed among the Eri silk fibers from different strains or in comparison to general *S. ricini* silk fibers when considering functional groups and crystallinity, specifically the crystalline β-sheet structure. Novel strains of *S. ricini* produce silk fibers comparable to commercial fibers, allowing for broader utilization in the textile industry and biomaterial applications.

Conflicts of interest

The authors declare that there is no conflict of interest in the research results or publication.

Acknowledgments

The authors are grateful to the IPB University for providing funding through the Young Lecturer Research scheme (11066/IT3.D10/PT.01.02/M/B/ 2023) to carry out this research.

References

[1] Vaidya, S.; Yadav, U. Rearing performance of *Philosamia ricini* (Eri silkworm) in different seasons of Ujjain district. *Environ. Conserv. J.* **2014**, *15* (3), 109–113. https://doi.org/10.36953/ecj.2014.15317.

[2] Borah, R. R.; Saikia, M.; Saikia, H.; Borgohain, A.; Borah Dutta, R. Seasonal variation in larval growth of Eri silkworm (*Samia ricini* Boisduval) reared on two Ailanthus species. *Environ. Conserv. J.* **2021**, *22* (1&2), 199–204. https://doi.org/10.36953/ecj.2021.221228.

[3] El-Sayed, H.; Taleb, M. A.; Mowafi, S. Potential applications of textile wastes and by-products in preparation of textile auxiliaries. *Egypt. J. Chem.* **2021**, *64* (8), 4433–4447. https://doi.org/10.21608/ejchem.2021.79398.3899.

[4] Silva, S. S.; Oliveira, N. M.; Oliveira, M. B.; Da Costa, D. P. S.; Naskar, D.; Mano, J. F.; Kundu, S. C.; Reis, R. L. Fabrication and characterization of Eri silk fibers-based sponges for biomedical application. *Acta Biomater.* **2016**, *32*, 178–189. https://doi.org/10.1016/j.actbio.2016.01.003.

[5] Market Data Research. *Silk Market Is Segmented by Type-Mulberry Silk, Tassar Silk, Eri Silk, Muga Silk, Application-Textile, Cosmetics, Medical & Region-North America, Europe, Asia Pacific, Latin America, Middle East and Africa - Global Industry Analysis on Size, Share, Growth*; 2023. https://www.marketdataforecast.com/market-reports/silk-market (accessed 2023-05-20).

[6] Lalitha, N.; Singha, B. B.; Das, B.; Choudhury, B. Impact of climate change in prospects of Eri silkworm seed production in Assam- A Review. **2020**, *5* (1), 10–14.

[7] Chutia, P.; Kumar, R.; Khanikar, D. P. Host plants relationship in terms of cocoon colour and compactness of Eri silkworm (*Samia ricini*). *Biol. Forum – An Int. J.* **2014**, *6* (2), 340–343.

[8] Narzary, F.; Brahma, D. Effect of different seasons on the rearing of Eri silkworm , *Samia ricini* on *Gmelina arborea* leaves. *J. Entomol.*

Zool. Stud. **2022**, *9* (4), 89–92.

[9] Andadari, L.; Yuniati, D.; Supriyanto, B.; Murniati; Suharti, S.; Widarti, A.; Steven, E.; Sadapotto, A.; Winarno, B.; Minarningsih; Agustarini, R.; Muin, N.; Isnan, W.; Heryati, Y.; Adalina, Y.; Yeny, I.; Dewi, R.; Nurlia, A.; Riendriasari, S. D.; Maharani, K. E.; Nugraha, L. M.; Narendra, B. H. Lens on tropical sericulture development in Indonesia: recent status and future directions for industry and social forestry. *Insects* **2022**, *13* (10), 1–25. https://doi.org/10.3390/insects13100913.

[10] Noor, R. R. Metode optimasi galur sintetik ulat sutera non murbei *Samia cynthia ricini* untuk wilayah marjinal. S00202300801, 2023.

[11] Sharma, P.; Kalita, J. C. Comparative study on tensile properties of silk fibres of different eri silk worm strains, *Samia ricini* (Donovan). *An Int. J. Environ. Biodivers.* **2017**, *8* (2), 121–123.

[12] Jao, D.; Mou, X.; Hu, X. Tissue regeneration: a silk road. *J. Funct. Biomater.* **2016**, *7* (3), 22. https://doi.org/10.3390/jfb7030022.

[13] Endrawati, Y. C.; Solihin, D. D.; Suryani, A.; Darmawan, N.; Suparto, H.; Rahmantika, B. Optimization of silkworm sericin extraction *Attacus atlas* and *Samia cynthia ricini* using response surface methodology. *Agritech* **2023**, *43* (1), 64–73.

[14] Oduor, E. O.; Ciera, L.; Adolkar, V.; Pido, O. Physical characterization of Eri silk fibers produced in Kenya. *J. Nat. Fibers* **2021**, *18* (1), 59–70. https://doi.org/10.1080/15440478.2019.1612306.

[15] Dawood, H. I.; Alshemary, K. K. H.; Mohammad, A. K.; Sabeeh, N. S. Microstructure, thermal, and mechanical properties of friction stir welded 6061 aluminum alloy with 10% SiCp reinforcement. *Egypt. J. Chem.* **2022**, *65* (4), 19–28. https://doi.org/10.21608/EJCHEM.2021.110858.5053.

[16] Fang, G.; Sapru, S.; Behera, S.; Yao, J.; Shao, Z.; Kundu, S. C.; Chen, X. Exploration of the tight structural-mechanical relationship in mulberry and non-mulberry silkworm silks. *J. Mater. Chem. B* **2016**, *4* (24), 4337–4347. https://doi.org/10.1039/c6tb01049k.

[17] Mazzi, S.; Zulker, E.; Buchicchio, J.; Anderson, B.; Hu, X. Comparative thermal analysis of Eri, Mori, Muga, and Tussar silk cocoons and fibroin fibers. *J. Therm. Anal. Calorim.* **2014**, *116* (3), 1337–1343. https://doi.org/10.1007/s10973-013-3631-0.

[18] Rockwood, D. N.; Preda, R. C.; Yücel, T.; Wang, X.; Lovett, M. L.; Kaplan, D. L. Materials fabrication from *Bombyx mori* silk fibroin. *Nat. Protoc.* **2011**, *6* (10), 1612–1631. https://doi.org/10.1038/nprot.2011.379.

[19] Yazawa, K.; Tatebayashi, Y.; Kajiura, Z. Eri silkworm spins mechanically robust silk fibers regardless of reeling speed. *J. Exp. Biol.* **2022**, *225* (3). https://doi.org/10.1242/jeb.243458.

[20] Malay, A. D.; Sato, R.; Yazawa, K.; Watanabe, H.; Ifuku, N.; Masunaga, H.; Hikima, T.; Guan, J.; Mandal, B. B.; Damrongsakkul, S.; Numata, K. Relationships between physical properties and sequence in silkworm silks. *Sci. Rep.* **2016**, *6* (January), 1–11. https://doi.org/10.1038/srep27573.

[21] Hossain, S.; Ali, R.; Hasan, T. Extraction and characterization of sericin from cocoon of four different silkworm races *Bombyx mori* L. *Eur. J. Adv. Chem. Res.* **2023**, *4* (3), 45–52. https://doi.org/10.24018/ejchem.2023.4.3.134.

[22] Alabadi, M. A.; Thahab, S. M.; Alshaibani, I. J. The effect of addition nanosilica on mechanical properties of poly (methyl methacrylate). *Egypt. J. Chem.* **2022**, *66* (8), 339–345. https://doi.org/10.21608/ejchem.2022.120635.5419.

[23] Hossein, H. A.; Youssef, H. F. Effects of synthetic hierarchical NaP-zeolite addition on physico-mechanical properties of OPC hydration development. *Egypt. J. Chem.* **2023**, *66* (5), 1–14. https://doi.org/10.21608/ejchem.2022.123935.5531.

[24] Dutta, S.; Talukdar, B.; Bharali, R.; Rajkhowa, R.; Devi, D. Fabrication and characterization of biomaterial film from gland silk of Muga and Eri silkworms. *Biopolymers* **2013**, *99* (5), 326–333. https://doi.org/10.1002/bip.22168.

[25] Muthumanickkam, A.; Subramanian, S.; Goweri, M.; Sofi Beaula, W.; Ganesh, V. Comparative study on Eri silk and mulberry silk fibroin scaffolds for biomedical applications. *Iran. Polym. J. (English Ed.* **2013**, *22* (3), 143–154. https://doi.org/10.1007/s13726-012-0113-3.

[26] Freddi, G.; Tsukada, M.; Berreta, S. Structure and physical properties of silk fibroin/Polyacrylamide blend films. *J. Appl. Polym. Sci.* **1999**, *71*, 1563–1571. https://doi.org/10.2115/fiber.39.10_P353.

[27] Lu, Q.; Hu, X.; Wang, X.; Kluge, J. A.; Lu, S.; Cebe, P.; Kaplan, D. L. Water-insoluble silk films with silk I structure. *Acta Biomater.* **2010**, *6* (4), 1380–1387. https://doi.org/10.1016/j.actbio.2009.10.041.

[28] Freddi, G.; Pessina G.; Tsukada M. Swelling and dissolution of silk fibroin (*Bombyx mori*) in N-methylmorpholine N-oxide. *Int. J. Biol. Macromol.* **1999**, *24*, 251.

[29] Mateab, S. H.; Albozahid, M. Study the effect of adding MWCNTs on the hardness, impact strength, and structural properties of composite materials based on epoxy polymer. *Egypt. J. Chem.* **2022**, *65* (3), 147–152. https://doi.org/10.21608/ejchem.2021.88640.4262.

[30] Rajkhowa, R.; Wang, L.; Kanwar, J. R.; Wang, X. Molecular weight and secondary structure change in Eri silk during alkali degumming and powdering. *J. Appl. Polym. Sci.* **2009**, *119*, 1339–1347. https://doi.org/10.1002/app.

[31] Lee, M.; Kwon, J.; Na, S. Mechanical behavior comparison of spider and silkworm silks using molecular dynamics at atomic scale. *Phys. Chem. Chem. Phys.* **2016**, *18* (6), 4814–4821. https://doi.org/10.1039/c5cp06809f.

[32] Zhang, S.; Tso, I.-M. Spider silk: factors affecting mechanical properties and biomimetic applications. *Extracell. Compos. Matrices Arthropods* **2016**, 489–513. https://doi.org/10.1007/978-3-319-40740-1.

[33] Vyas, S. K.; Shukla, S. R. Comparative study of degumming of silk varieties by different techniques. *J. Text. Inst.* **2016**, *107* (2), 191–199. https://doi.org/10.1080/00405000.2015.1020670.